# Geomagnetic Research From Space

PAGES 213–214

The Decade of Geopotential Field Research, inaugurated in 1999 with the launch of the Danish satellite Ørsted on 23 February, was designed as an international effort to promote and coordinate continuous monitoring of geopotential field variability in the near-Earth environment. Since 1999, the Challenging Minisatellite Payload (CHAMP), the Gravity Recovery and Climate Experiment (GRACE), the Satélite de Aplicaciones Científicas-C (SAC-C), and most recently, the Gravity field and steady-state Ocean Circulation Explorer (GOCE) satellites have combined with Ørsted to generate an unprecedented wealth of data on Earth's magnetic and gravity fields.

Interpretation of the new magnetic data from the Decade has led to improvements in scientists' knowledge of the fast changing small scales of the Earth's magnetic field, providing details of magnetic field generation within the Earth's core. The new magnetic data have also been used in the World Digital Magnetic Anomaly Map (WDMAM) project, which "images" the lithosphere's igneous and metamorphic rocks. Such data, associated theory, and modeling work also led to the discovery of previously undetected processes with magnetic signatures that can be observed by satellites, including oceanic tides, ionospheric pressure gradient currents and ionospheric plasma irregularities, and serpentinized mantle overlying subduction zones. Knowledge of the magnetic properties of these processes provides scientists with a new perspective of the physics involved in the phenomena.

CHAMP, one of the main data collectors for the Decade, may reenter the atmosphere by the end of 2009, depending on solar activity. CHAMP will be succeeded by Swarm, the fifth Earth Explorer mission in the European Space Agency's Living Planet Programme (Figure 1a). The new mission aims to measure the Earth's magnetic field with unprecedented accuracy through a constellation of three polar-orbiting satellites, designed to maximize the scientific return in the areas of core dynamics, lithospheric magnetization, and three-dimensional (3-D) mantle conductivity. It will also investigate electric currents flowing in the magnetosphere and ionosphere, quantify satellite drag in the upper atmosphere, and search for the magnetic signature of ocean circulation.

The Decade has given geomagnetic research endeavors a strong foundation. Swarm will build on these past accomplishments and usher in a new era in the study of geomagnetism through separating the multitude of sources contributing to the Earth's magnetic field.

## *Understanding the Effects of Internal Magnetic Fields*

The sources of the Earth's magnetic field fall into two categories: The field is generated either from electric currents or from magnetized material. Electric currents can be found throughout the Earth system. The largest of these current systems is found inside the metallic core, but smaller current systems exist within the ionosphere, magnetosphere, and oceans. The current systems within the Earth's core are generated by a self-sustaining dynamo process and are closely tied to motions in the liquid metal outer core. Two main types of instruments are used to detect the geomagnetic field: fluxgate magnetometers, for measuring the direction of the field, and scalar magnetometers, for measuring its magnitude.

To learn more, scientists have recently looked to Mercury, the only other terrestrial planet besides the Earth with a planet-wide intrinsic magnetic field. Two recent flybys of the Sun's innermost planet by NASA's Mercury Surface, Space Environment, Geochemistry, and Ranging (MESSENGER) spacecraft have revealed that the large-scale morphology of Mercury's internal magnetic field [*Anderson et al.*, 2008] is similar to that of Earth's, although Mercury's surface field is 2 orders of magnitude weaker. Dominantly dipolar and spin-aligned, the fields of both planets possess significant nondipole moments, manifested as polar and equatorial magnetic "lows." In the case of Earth, the "low" is referred to as the South Atlantic

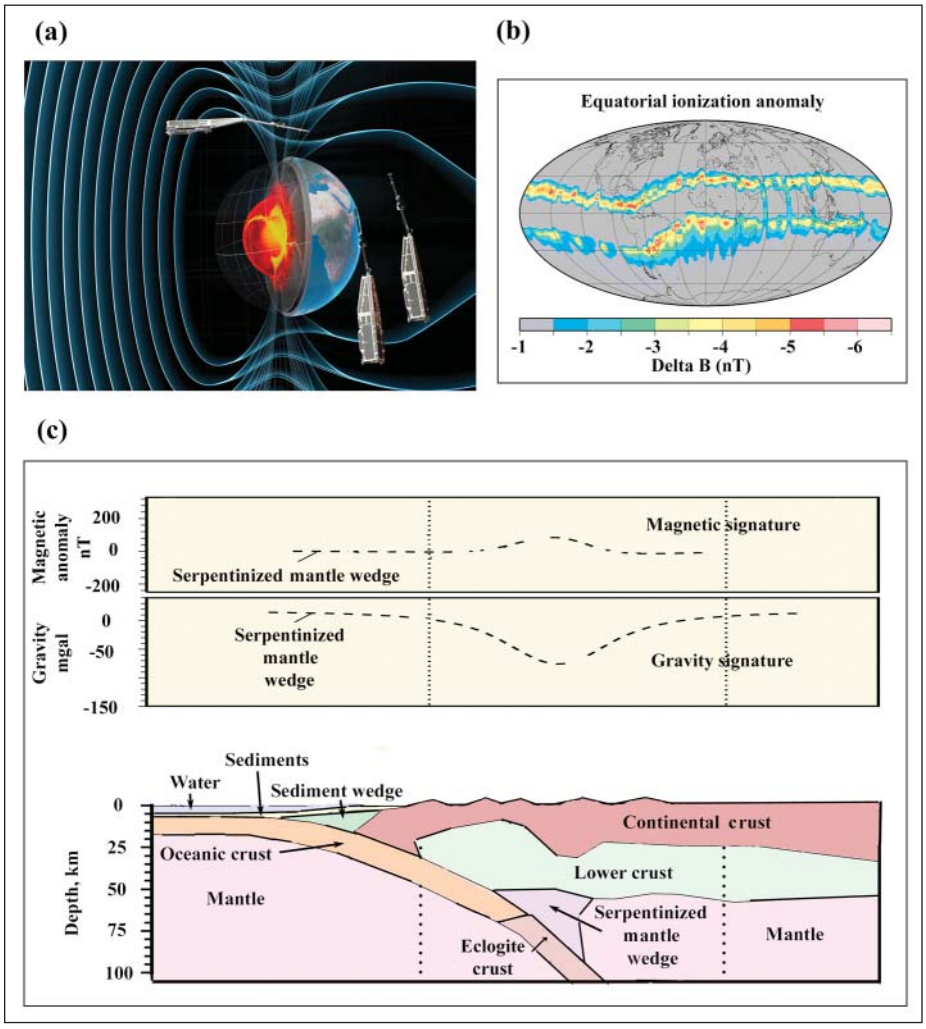


*Fig. 1. (a) Schematic of the upcoming Swarm constellation, set within the geomagnetic environment of the Earth. Image courtesy of the European Space Agency (ESA)/Advanced Operations and Engineering Services (AOES) Medialab. (b) Magnetic effect of the equatorial ionization anomaly after sunset at 400 kilometers in altitude, from 23 to 27 October 2001 [*Lühr et al., *2003]. The color bar represents the change in magnetic field* B, *measured in nanoteslas. (c) Crust and upper mantle model of subduction zone and related serpentinite mantle wedge associated with magnetic and gravity anomalies, the latter measured in milligals. Adapted from* Blakely et al. *[2005].*

By E. Friis-Christensen, H. Lühr, G. Hulot, R. Haagmans, and M. Purucker

anomaly, a region marked by a growing reverse flux patch on the top layer of the underlying core.

The South Atlantic anomaly is an oval-shaped geographic region in the southern Atlantic Ocean east of Brazil. Because of the relatively weak magnetic field here, particles from the Van Allen radiation belts have access to lower altitudes, and the associated increased radiation dose adversely affects satellites traveling through the region. This feature has existed since at least 1840 and is closely tied to the overall decrease of the strength of the Earth's dipole (5% per century) since that time [*Jackson and Finlay,* 2007]. Another large-scale phenomenon is the rapid motion of the north magnetic dip pole (where the field direction is vertical). Because the horizontal component of the magnetic field in the region of this pole exhibits a very flat gradient, small changes in the field can cause significant displacements of the pole [*Mandea and Dormy,* 2003].

What causes such changes in the field? Changes of internal origin can now be witnessed with unprecedented space and time resolution, providing detailed pictures of fast changing small-scale structures in the field produced within the core [*Hulot et al.,* 2002, 2007]. The dynamics of these features have been shown to affect the length-of-day variation and may testify to unexpectedly rapid flow changes in the Earth's core [*Olsen and Mandea,* 2008], a provocative suggestion that needs further validation from the Swarm mission.

### *Magnetic Anomalies*

Although the magnetic fields from the Earth's core represent some 99% of the Earth's magnetic field, material in the crust and uppermost mantle produces fields that are easily measurable with sensitive magnetometers. This material is magnetized and is dominantly associated with igneous and metamorphic rocks rich in iron oxides, although sedimentary rocks also have subordinate but measurable magnetism. This magnetism is a function of temperature; rocks lose their magnetism as they approach their Curie temperature, typically 200º–700ºC.

Studies of crustal magnetism have contributed to geodynamic models of the lithosphere, geologic mapping, and petroleum and mineral exploration. Maps of crustal magnetic fields, interpreted in conjunction with other information, have been used to locate diamond-bearing kimberlites and meteorite impacts. The depth of the magnetized rocks can be inferred by mapping the wavelength of the magnetic fields, with the deepest sources producing the longest wavelengths.

Using sensitive magnetometers on board satellites, airplanes, and ships, crustal magnetic fields have been mapped in the Magnetic Anomaly Map of the World, published in 2007 by the WDMAM project [*Korhonen et al.,* 2007]. The map represents the first global compilation of the wealth of magnetic anomaly information and was generated by combining CHAMP satellite data and aeromagnetic and seagoing surveys, supplemented by anomaly values estimated from a combination of oceanic crustal ages and a magnetic polarity timescale. Because information is collected from ground-based and satellite-based surveys, large-scale patterns and fine-scale fluctuations can be observed. A new generation of the map is planned for 2011 and will include many new data from oceangoing surveys, although the southern oceans still remain poorly surveyed.

The Earth's mantle is usually considered to be nonmagnetic because of mineralogy and elevated temperature, but investigations conducted during the Decade of Geopotential Field Research reveal that subduction margins may be an exception to this rule. Subducting oceanic slabs release water into overlying continental mantle, thereby transforming peridotite into serpentinite. Serpentinite often contains abundant magnetite, and thermal models suggest that cold, descending slabs cool the mantle to below the Curie temperature of magnetite, revealing its magnetic signature. Magnetic and gravity anomalies over subduction zones are commonly seen in satellite maps, and in the Cascadia and Alaskan subduction zones, for example, the depth of the sources of these long-wavelength anomalies has been estimated to lie within the mantle (Figure 1c; see also *Blakely et al.* [2005]).

### *Magnetic Signatures of Oceanic Tides*

Newly recognized processes with satellite magnetic signatures also include the oceanic lunar semidiurnal ($M_2$) tide [*Tyler et al.,* 2003]. The semidiurnal tide possesses a magnetic signature because seawater is an electrically conducting fluid. The flow of this fluid through the Earth's main magnetic field in turn generates magnetic fields, but these do not affect the tidal flow to any significant degree.

The tidal signature was easily recognized because of a clear $M_2$ peak in the intensity spectra over the ocean data collected by CHAMP, in contrast to the land data where the peak was absent. Additionally, a global numerical prediction of these magnetic fields was in good agreement with observations. Of more importance for climate modeling, the magnetic signal associated with oceanic currents should be measurable by CHAMP, and soon by Swarm. However, the spatial scale of these signals overlaps with those from the core and crust, and they have not yet been isolated.

### *Complications to Measurements*

Complicating satellites' ability to isolate the Earth's internal magnetic fields are a variety of magnetic fields from sources above the neutral atmosphere in the region called geospace, several of which have been recognized for the first time as a consequence of high-resolution magnetometers and plasma instrumentation on CHAMP. Examples include the magnetic fields associated with regions of dense plasmas [*Lühr et al.,* 2003] or irregularities within the equatorial ionosphere [*Stolle et al.,* 2006], as well as with gravity-driven electric currents in the ionosphere [*Maus and Lühr,* 2006].

Electron density anomalies are prominent north and south of the magnetic equator, especially after sunset. These lead to magnetic field depletions of only one part in 10,000 (Figure 1b), which explains why they were not previously recognized. The magnitude and scale size of these features fall within the range of crustal anomalies, and earlier models of the crustal magnetic field often contained spurious signatures skewed by electron density anomalies. These features can also cause artifacts in main field models, especially in the secular variation and acceleration coefficients, due to the effect's dependence on the 11-year solar cycle.

Because the Swarm satellites will be at two different local times, external field effects and corresponding induced effects are more likely to be recognized and isolated. Extensive simulation studies have shown how satellites at multiple local times can be optimized to do the best job of separating internal, external, and induced fields.

### *Looking to the Future*

New discoveries of processes through analysis of satellite magnetic signatures are expected to continue apace with Swarm. Swarm's constellation will include two spacecraft at low altitude, measuring the east-west gradient of the magnetic field, and one at higher altitude in a different orbital plane. The new satellites will carry instrumentation to measure the vector and scalar magnetic fields, electric fields and plasma parameters, nongravitational accelerations, and position (with the Global Positioning System). In addition, by making it possible to access the detailed evolution of the field at the top layer of the underlying core over a significant time period, data assimilation procedures may be used to predict the future behavior of the Earth's magnetic field.

Work on prediction already has begun, with promising results [*Fournier et al.,* 2007; *Liu et al.,* 2007]. The improved local time coverage of the Swarm satellites will significantly advance studies of the 3-D electrical conductivity of the mantle. Conductivity variations often correspond to large-scale variations in water content, and this approach could complement seismic techniques for imaging subducted slabs within the mantle. Finally, the magnetic signature of subduction and serpentinization will allow for detailed study of the possible connection between intraslab earthquakes and the hydrated fore-arc mantle [*Blakely et al.,* 2005].

Expected results from Swarm and new results from CHAMP and Ørsted will be

presented at the Second Swarm International Science Meeting, to be held at the German Research Centre for Geosciences (Deutsches GeoForschungsZentrum (GFZ)), in Potsdam, Germany, from 24 to 26 June 2009. For more information on geomagnetic research and its applications, please visit http://www.esa.int/esaLP/LPswarm.html.

*Acknowledgments*

We would like to acknowledge Richard Blakely, Eric Donovan, and two anonymous reviewers for very helpful suggestions.

*References*

Anderson, B. J., M. H. Acuña, H. Korth, M. E. Purucker, C. L. Johnson, J. A. Slavin, S. C. Solomon, and R. L. McNutt (2008), The structure of Mercury's magnetic field from MESSENGER's first flyby, *Science, 321,* 82–85.

Blakely, R. J., T. M. Brocher, and R. E. Wells (2005), Subduction-zone magnetic anomalies and implications for hydrated forearc mantle, *Geology, 33,* 445–448.

Fournier, A., C. Eymin, and T. Alboussiere (2007), A case for variational geomagnetic data assimilation: Insights from a one-dimensional, nonlinear, and sparsely observed MHD system, *Nonlinear Processes Geophys., 14,* 163–180.

Hulot, G., C. Eymin, B. Langlais, M. Mandea, and N. Olsen (2002), Small-scale structure of the geodynamo inferred from Ørsted and Magsat satellite data, *Nature, 416,* 620–623.

Hulot, G., T. Sabaka, and N. Olsen (2007), The present field, in *Treatise on Geophysics*, vol. 5, *Geomagnetism,* edited by M. Kono, pp. 33–75, Elsevier, New York.

Jackson, A., and C. C. Finlay (2007), Geomagnetic secular variation and its applications to the core, in *Treatise on Geophysics*, vol. 5, *Geomagnetism,* edited by M. Kono, pp. 147–193, Elsevier, New York.

Korhonen, J., et al. (2007), Magnetic anomaly map of the world, Comm. for the Geol. Map of the World, Paris.

Liu, D., A. Tangborn, and W. Kuang (2007), Observing system simulation experiments in geomagnetic data assimilation, *J. Geophys. Res., 112,* B08103, doi:10.1029/2006JB004691.

Lühr, H., M. Rother, S. Maus, W. Mai, and D. Cooke (2003), The diamagnetic effect of the equatorial Appleton anomaly: Its characteristics and impact on geomagnetic field modeling, *Geophys. Res. Lett., 30*(17), 1906, doi:10.1029/2003GL017407.

Mandea, M., and E. Dormy (2003), Asymmetric behavior of magnetic dip poles, *Earth Planets Space, 55,* 153–157.

Maus, S., and H. Lühr (2006), A gravity-driven electric current in the Earth's ionosphere identified in CHAMP satellite magnetic measurements, *Geophys. Res. Lett., 33,* L02812, doi:10.1029/2005GL024436.

Olsen, N., and M. Mandea (2008), Rapidly changing flows in the Earth's core, *Nat. Geosci., 1,* 390–394.

Stolle, C., H. Lühr, M. Rother, and G. Balasis (2006), Magnetic signatures of equatorial spread *F* as observed by the CHAMP satellite, *J. Geophys. Res., 111,* A02304, doi:10.1029/2005JA011184.

Tyler, R. H., S. Maus, and H. Lühr (2003), Satellite observations of magnetic fields due to ocean tidal flow, *Science, 299,* 239–241.

*Author Information*

Eigil Friis-Christensen, National Space Institute, Technical University of Denmark, Copenhagen, Denmark; E-mail: efc@space.dtu.dk; Hermann Lühr, German Research Centre for Geosciences (Deutsches GeoForschungsZentrum (GFZ)), Potsdam, Germany; Gauthier Hulot, Institut de Physique du Globe de Paris, Paris, France; Roger Haagmans, European Space Agency, Noordwijk, Netherlands; and Michael Purucker, Raytheon at NASA Goddard Space Flight Center, Greenbelt, Md.

# Unique Meteorological Data During Hurricane Ike's Passage Over Houston

PAGE 215

Hurricane Ike passed over the Houston, Tex., metropolitan area during the early morning of 13 September 2008. Although Ike had been rated only a category 2 on the Saffir-Simpson scale at landfall near Galveston, Tex., the storm's widespread damage to urban trees, many lacking proper trimming, knocked out the area's power distribution system; for some customers, power was only restored a month later.

The hurricane's path after landfall (Figure 1a) went north through Galveston Bay and Baytown. The city of Houston—with its economically important ship channel—experienced the less severe western eye wall, the tight circulation with maximum wind speeds around the hurricane's center. The eye's passage was recorded between 3:00 and 4:30 A.M. Central Standard Time (CST; Figures 1a and 1c). It had maintained its unusually large diameter of 35–40 kilometers in its first hours after landfall.

Characteristics of land-falling hurricanes have been recorded previously [e.g., *Lorsolo et al.,* 2008; *Skwira et al.,* 2005] but not over urban terrain. Data recorded at two elevated meteorological stations in Houston may be able to shed light on why Ike's winds were so devastating.

## *Hurricane Ike in Urban Houston*

Urban surfaces are aerodynamically rougher than most natural surfaces [*Roth,* 2000], creating increased friction and shear, including many small-scale wakes from individual structures [*Klipp,* 2007]. To demonstrate the hurricane's force in the urban environment, meteorological data were used from a Texas A&M University project located at a commercial, lattice-structure communications tower owned by the Houston Yellow Cab company (HYC; 29.789°N, 95.354°W, 14 meters above sea level (asl); Figure 1b), with sensors up to 60 meters above ground level (agl); and from a University of Houston (UH) project located atop the university's northern Moody Towers building (29.718°N, 95.341°W, 11 meters asl, 76 meters agl).

At the HYC tower, data were recorded in 10-second intervals and were stored as 1-minute averages and standard deviations; atmospheric pressure data were recorded every 15 minutes. While some sensors were lost, wind data from the top level, installed north of the tower structure, were unaffected. The four lower-level cup anemometers, installed south of the tower, recorded reduced speeds during northerly winds. Rainfall and pressure were recorded at 12 and 2 meters agl.

The UH measurements included 10-second samples of pressure, temperature, humidity, wind speed, and direction.

Figure 1c shows pressures and accumulated rainfall, and Figures 1d and 1e show 1-minute mean winds (sustained winds) and 10-minute mean winds at the 60-meter level on the HYC tower (Figure 1d) and at 76 meters agl on the UH tower mast, respectively. Maximum sustained wind speeds exceeded 30 meters per second (67 miles per hour (mph)) when the eye of the hurricane was located east of the HYC site. Peak 10-second gusts were estimated to have ranged from 34 to 36 meters per second (80 mph). Maximum rain rates in the hurricane's inner rainbands were 40 millimeters per hour, with peak values of 1.25 millimeters per minute. The lowest pressure, 960 millibars, was recorded slightly later at the HYC than at the UH site, as expected from the hurricane's northerly path (Figure 1a). Maximum sustained wind speeds of 32 meters per second (72 mph) were recorded at the UH site, with peak 10-second gusts exceeding 38 meters per second (85 mph), on the southwest side of the eye with winds advecting over relatively flat terrain toward the building.

## *Wind Damage and Turbulence*

Wind damage to structures arises from static and dynamic, or gust, wind loads [*Plate and Kiefer,* 2001]. Because of friction-induced gustiness, the wind damage potential is likely larger to trees in an urban environment than to those in undisturbed forests. Measurements and modeling of wind damage potential to remaining trees in logged forests [e.g., *Ancelin et al.,* 2004; *Panferov and Sogachev,* 2008; *Zeng et al.,* 2009] have shown that aside from the static wind load (proportional to the sustained wind speed squared), dynamic wind load due to turbulence can be critical. Turbulent kinetic energy (TKE) in hurricanes is dominated by shear production, proportional to the square of the friction velocity ($u^{*2}$). The effect of TKE on wind loads grows much more rapidly with wind speed than with static load [*Panferov and Sogachev,* 2008].